Pergamon

Journal of Structural Geology, Vol. 16, No. 9, pp. 1217 to 1231, 1994

0191-8141/94 $07.00+0.00

0191-8141(93)E0029-K

On volume change and mass transport during the development of crenulation cleavage

NEIL S. MANCKTELOW

Geologisches Institut, ETH-Zentrum, CH-8092 Zürich, Switzerland

(*Received* 7 *July* 1993; *accepted in revised form* 1 *December* 1993)

Abstract—A comparison of the bulk chemistry between isolated zones of crenulation cleavage and the surrounding relatively homogeneous slates from three localities (Boscastle, SW England; Moselle Valley, Germany; Lac de Roselend, French Alps) demonstrates that marked bulk volume change is not a prerequisite for the development of crenulation cleavage. X-ray powder diffraction results also demonstrate that there is no significant mineralogical change between crenulated and uncrenulated zones for the samples studied. Mineralogical differentiation and mass transfer takes place on a local scale between the limb and hinge domains of individual crenulation folds and of larger scale folds in layering, but can occur without significant overall volume change on the scale of crenulated zones containing many microlithon and cleavage domains. Relative volume changes between crenulated and uncrenulated regions do not exceed *ca* 5% at Boscastle and the majority of samples from the Moselle Valley. At one locality in the Moselle Valley, however, a volume loss of around 35–40% occurred from the crenulated zone, produced almost entirely by loss of SiO_2 (as quartz) from the system. Isolated parallel-sided bands of crenulation cleavage, such as the examples from Boscastle and the Moselle Valley, are geometrically constrained to represent some combination of volume change and heterogeneous simple shear, superimposed upon a background homogeneous strain. In examples with minimal volume changes, the heterogeneous strain component must be one of simple shear.

INTRODUCTION

CRENULATION cleavage is the most common form of cleavage observed in multiply deformed rocks (e.g. Leith 1905, Knill 1960, Rickard 1961, Borradaile *et al.* 1982). Its development relies on the presence of a pre-existing, well-developed foliation (e.g. Hoeppener 1956, Rickard 1961, Talbot 1964): this foliation is usually an earlier tectonic cleavage, but in some cases the sedimentary compaction fabric parallel to bedding may be sufficiently strong that the first tectonic cleavage itself has the morphology of crenulation cleavage on a sub-microscopic scale (Weber 1981). Microfolding ('crenulation') of the earlier planar fabric is accompanied by mineralogical differentiation. As a result, the hinge region of the microfolds becomes enriched in the more 'soluble' components (calcite, quartz, feldspar) to form a generally lighter-coloured microlithon domain of grains with a weak shape preferred orientation fabric, whereas the limbs are enriched in the 'insoluble' components (phyllosilicates, opaques) to develop a dark cleavage domain of platy minerals with a strong shape preferred orientation, along which the rock preferentially breaks to form the characteristic, domainal crenulation cleavage (Nicholson 1966, Talbot & Hobbs 1968, Williams 1972, 1982, Cosgrove 1976, Gray 1977a,b, 1979, 1987, Marlow & Etheridge 1977, Gray & Durney 1979). It is clear from this observed mineralogical differentiation, as well as from published chemical analysis data (Cosgrove 1976, Gray 1977a, Marlow & Etheridge 1977), that there has been a mass transfer of chemical components on the wavelength scale of the microfolding. The approximately similar geometry of the microfolds also indicates that local volume changes have occurred, with an increase in volume in the hinge region relative to the limbs (Gray 1977a, Marlow & Etheridge 1977, Mancktelow 1982). The component minerals in zones of crenulation cleavage show little evidence of intragranular deformation, such as undulose extinction, subgrain formation or recrystallization (Gray 1977a, Marlow & Etheridge 1977), which suggests that the most important deformation mechanism is one of intergranular diffusion. Although it is now well accepted that diffusion and volume change are important on the scale of the microfolds themselves, it has not been established if an overall volume change generally accompanies the development of crenulation cleavage (e.g. Bell & Cuff 1989) or if material is only locally redistributed over the scale of several adjacent domains (e.g. Gray & Durney 1979, Mancktelow 1982).

Crenulation cleavage is commonly developed in isolated band-like zones within otherwise relatively homogeneous, though well-foliated, rocks (e.g. Talbot 1964). It should be possible, therefore, to compare the bulk whole-rock composition of the crenulated and uncrenulated material to establish if significant bulk volume change and chemical mass transport is generally involved in the development of crenulation cleavage. This has been the aim of the present study.

LOCATION AND DESCRIPTION OF SAMPLES

Boscastle

The two samples (Bosc-1 and Bosc-2, Figs. 1 and 2) were collected from the classic location for crenulation

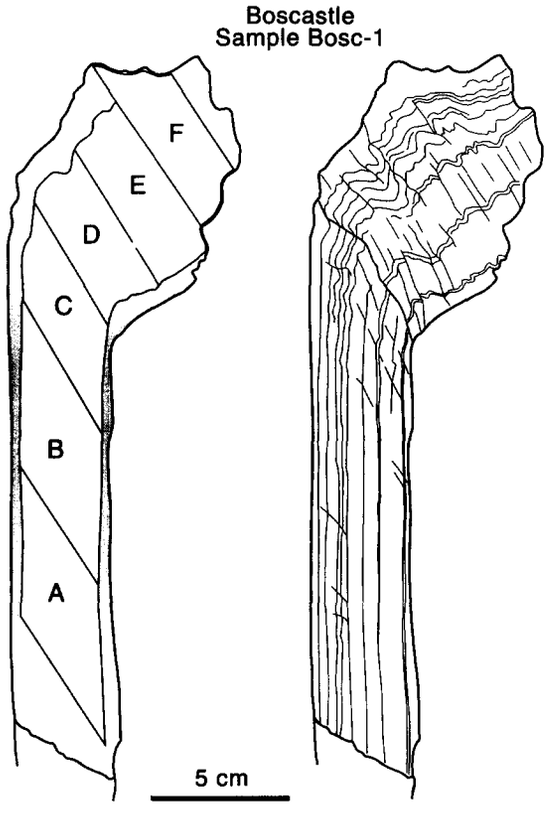

Fig. 1. Sketch of sample Bosc-1 (Fig. 5b), collected as a loose block at Penally Point, Boscastle, SW England (Dearman & Freshney 1966). A–F are the outlines of the small blocks (each *ca* 2 cm thick) which were analysed for major and minor elements.

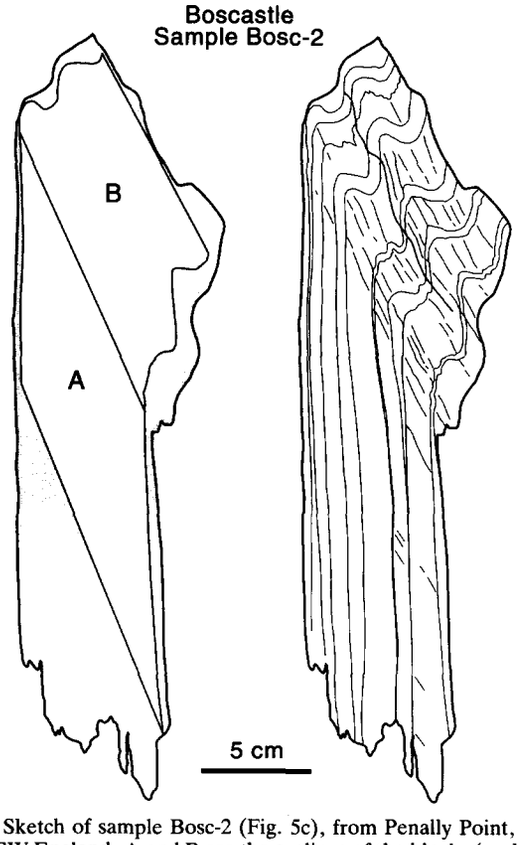

Fig. 2. Sketch of sample Bosc-2 (Fig. 5c), from Penally Point, Boscastle, SW England. A and B are the outlines of the blocks (each *ca* 2 cm thick) which were analysed for major and minor elements.

cleavage and overprinted folding at the mouth of Boscastle harbour in SW England (Dearman & Freshney 1966). Although the overall geometry is quite complex (*op. cit.*), excellent examples of narrow (10–20 cm) parallel-sided bands of crenulation cleavage developed within planar-foliated argillaceous black slates of quite homogeneous composition can be found both in place (Fig. 5a) and as loose specimens (Figs. 5b & c), which were collected in preference to destroying unique outcrops. The samples were serially sectioned, photographed and then divided into blocks delimited on two sides by the same fine compositional bands (almost certainly bedding, now parallel to the pervasive first cleavage) and on the other two sides by planes parallel to the new, axial-planar crenulation cleavage (Figs. 1 and 2). The blocks should, therefore, all represent the same initial bedding package prior to crenulation and initial composition variation along this bedding package in these relatively homogeneous slates should be minor. (This is indeed confirmed by the analyses, as will be seen below.) In the sample Bosc-1, a total of six small samples were taken in a traverse from the uncrenulated (or very weakly crenulated) region of planar foliation into the strongly crenulated region (Fig. 1), to investigate the local variability parallel to bedding both in the initial composition (Bosc-1A and B) and within the crenulated zone itself (Bosc-1C, D, E and F). In the second sample Bosc-2, only two larger blocks were analysed (Fig. 2): one from the uncrenulated region (Bosc-2A) and an adjacent one from the crenulated zone (Bosc-2B), to provide smoothed averages for a larger volume of material from the two zones.

Moselle Valley

The samples come from another classic region for crenulation cleavage, namely the Hunsrückschiefer of the middle Moselle region, Germany, where the existence of isolated bands of crenulation cleavage in otherwise relatively homogeneous argillaceous slates has been described by Talbot (1964). Samples were collected from two localities. Hun-1 and Hun-2 both come from a small disused quarry 2 km southeast of Bernkastel (map co-ordinates 790/302), and like the samples from Boscastle were collected from adjacent crenulated and uncrenulated (or very weakly crenulated) planar-foliated domains (Figs. 3 and 5g). Again blocks were cut such that they were bounded on two sides by the folded earlier cleavage, and on the other two sides by planes parallel to the new crenulation cleavage (Fig. 3). The second locality is on the left bank of the Moselle River opposite Leiwen (map co-ordinates 638/215). Here, a narrow band of intense crenulation cleavage transects the otherwise weakly crenulated slates (Figs. 6a & b). Collecting a single sample across the boundary was not possible. In this case two separate samples, one from the weakly crenulated material (Hun-3) and one from the crenulation cleavage zone (Hun-4, Fig. 6b) were collected and analysed.

Lac de Roselend

The geometry of the samples from calcareous slates at the northeastern end of Lac de Roselend, in the external French Alps east of Beaufort (e.g. Tricart 1980, Spencer 1989), is different from those of the other two locations. The crenulation cleavage considered here (Figs. 4 and 6c) is developed as an axial planar cleavage in isolated intrafolial fold packets, which are surrounded by more planar foliated slates, rather than as elongate band-like zones. These fold packets have been produced where local flow perturbations (perhaps due to quite minor compositional variation or around small inclusions, e.g. Van den Driessche & Brun 1987) have caused a rotation of the dominant planar foliation through the shear plane during continued progressive shearing, placing it locally in an orientation of incremental shortening (Tricart 1980).

Several quite large (*ca* 1 kg) samples were taken: samples Ros-1, 3 and 6 represent weakly crenulated or uncrenulated material and Ros-2, 4 and 5 the strongly crenulated material (Fig. 4). The wavelength of the crenulations at this locality is around an order of magnitude larger (1.5–2 mm, Fig. 6d) than for samples from Boscastle or the Moselle Valley (0.1–0.2 mm, Figs. 5e, f & h and 6b). These samples provide an interesting comparison with the other two locations both because of the different geometry of the crenulation packets and because of the different chemistry: the samples from Lac de Roselend are calcite-rich in contrast to the quartz-rich, practically carbonate-absent mineralogy of the Boscastle and Moselle samples.

METHODS AND RESULTS

The whole-rock major and trace element analyses, determined by standard XRF techniques, are listed in the tables of the Appendix. Results from each of the localities will be considered separately before being compared and summarized in the discussion section below.

Two graphical methods have proved particularly useful in treating the raw analytical data. Both of these methods consider the basic problem that in any comparison of chemical composition between two samples there are two unknowns: the change in mass of a particular chemical component and the relative change in volume between the specimens. The plotting method of Gresens (1967) provides an elegant and clear way to present this comparison graphically. It can readily be shown that, for any metasomatic alteration of a rock A into a rock B, the changes in mass, volume and density are related according to the following equation (after Gresens 1967, equation 14):

$$X_n = X_B f_v \left(\frac{\rho_B}{\rho_A}\right) - X_A, \quad (1)$$

where X_n is the mass (in weight %) of a chemical component of interest gained or lost during the alteration of A into B, f_v is the volume factor (i.e. the ratio V_B/V_A = volume of rock B/volume of rock A), X_A is the weight % of the chemical component of interest in rock A, X_B is the weight % of the same component in rock B, and ρ_A and ρ_B are the respective densities of A and B. Measurements using standard pycnometer procedures

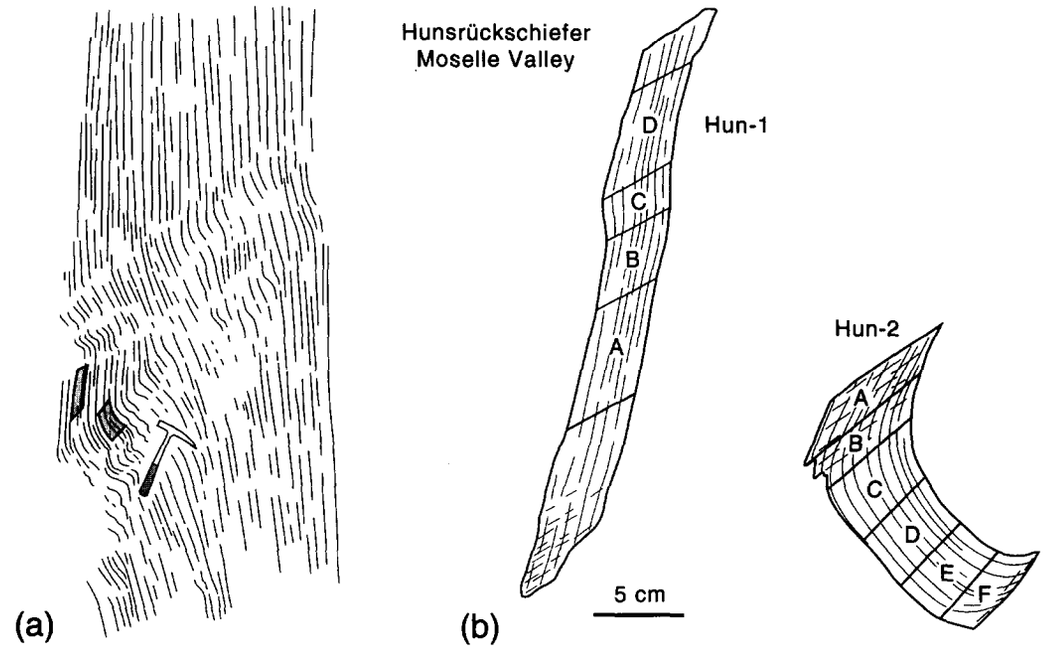

Fig. 3. Sketch of samples Hun-1 and Hun-2, collected from a quarry 2 km southwest of Bernkastel, Moselle Valley, Germany. (a) Sketch of outcrop (Fig. 5g) with location of samples indicated. Most of the outcrop has a single planar slaty cleavage fabric; the crenulation folds and associated crenulation cleavage only develop in isolated zones. (b) Orientation and spacing of samples collected. Hun-1 represents the generally planar slaty cleavage fabric, Hun-2 the crenulated zone. Letters refer to blocks (each *ca* 2 cm thick) which were analysed for major and minor elements.

(Hutchinson 1975) of uncrenulated and crenulated samples from Lac de Roselend (Ros-3, 5 and 6) have shown that the density variation is minimal (specific weight of all three samples in the range 2.75 ± 0.02); equation (1) can thus be simplified by assuming that the density ratio equals unity. For each analysed component, a linear plot of X_n (% mass change) against f_v (volume factor) can be constructed to produce a standard Gresens plot, such as Fig. 7(a). Immobile elements should all have $X_n \approx 0$ (i.e. no gain or loss of material) and the plotted lines for each of these elements should intersect each other on the '% mass change = 0' axis at the same volume factor—providing a method for estimating the volume change involved in the transformation of rock A into rock B. Since the slope of each of the plotted lines on the standard Gresens plot is equal to X_B, all minor components and particularly trace elements will have very low slopes compared to the major elements and will be difficult to differentiate from each other. A comparison of the compositional variation in both minor and major element abundances is better achieved using a normalized Gresens plot (e.g. Fig. 7b), as suggested by Potdevin & Marquer (1987). For this plot, both sides of equation (1) are divided by X_A (in other words, the relation is normalized against the amount of the particular component in rock A), resulting in the equation:

$$\frac{X_n}{X_A} = \frac{X_B}{X_A} f_v \left(\frac{\rho_B}{\rho_A}\right) - 1. \qquad (2)$$

In the normalized Gresens plot, immobile elements with $X_n \approx 0$ will cluster as a series of nearly coincident lines all crossing the 'normalized mass change = 0' axis at approximately the same value of the volume factor.

The second technique considers the ratio of one component relative to another. If a particular component is immobile, changes in its abundance in the chemical analyses can only reflect its passive concentration or dilution due to volume change. Two elements which are often taken to be effectively immobile are Al and Ti (e.g. Carmichael 1969), although the not uncommon occurrence of aluminosilicate-rich segregations during metamorphism warns that this need not always be the case (Mills 1964, Klein 1976). However, the very consistent ratio of TiO_2 to Al_2O_3 in all the samples (e.g. see Figs. 9 and 12) is certainly in accord with an immobile, passive behaviour of these elements in the current examples. If all other components are normalized against one of these immobile elements (Al_2O_3 is used here), then the effect of volume change is eliminated and the relative enrichment or depletion of other components due to mass diffusion can be considered directly. This approach is identical to assuming that the volume loss corresponds to that point on the Gresens plot where the Al_2O_3 line intersects the '% mass change = 0' axis (i.e. no mass diffusion of this element), and then considering the relative enrichment or depletion of all other elements along the vertical line corresponding to this specific volume loss. In this way, the Gresens or normalized Gresens plots allow a ready assessment of the probable volume change, whereas the plots of chemical component ratio against Al_2O_3 highlights the effect of mass diffusion. The two representations are thus complementary.

From the chemical analysis, it is also possible to calculate a theoretical mineral mode. Given the chemical composition of each major mineral present, the calculation is a least-squares linear programming problem and can readily be solved by standard methods. The calculated modes are useful for linking the measured chemical changes to the mineralogical differentiation which is observed in thin section.

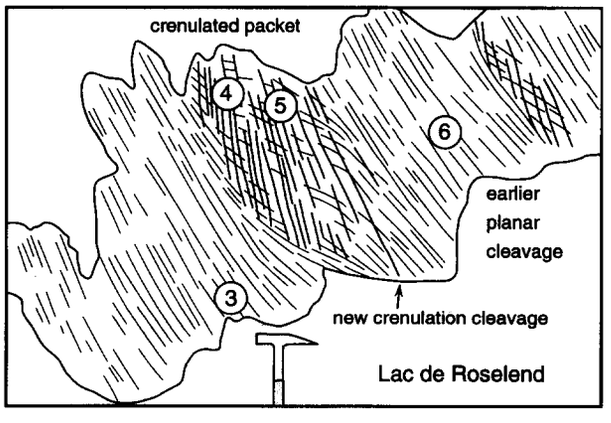

Fig. 4. Sketch of the outcrop at the northeastern end of Lac de Roselend in the French Alps near Beaufort (Fig. 6c). The location of samples Ros-3–6 are indicated. Samples Ros-1 (uncrenulated) and Ros-2 (crenulated) were taken from an outcrop *ca* 2 m for aesthetic reasons, perhaps close up to 'further left'.

Boscastle

The bulk-rock chemistry of the planar-foliated region of Bosc-1 A+B is compared to the strongly crenulated region Bosc-1 D+E in the standard and normalized Gresens plots of Fig. 7(a) & (b), respectively. These plots indicate that the overall mass and volume change between the two domains is small. If anything, there is a slight relative volume increase of ≤ 5% within the strongly crenulated hinge domain. This is close to the lower resolution limit of the technique, which is determined by the initial variability in bulk rock composition prior to crenulation. The slight volume increase is effected by an increase of 5–6 weight % in SiO_2, which only represents one-tenth of the total SiO_2 content. Very similar observations pertain to sample Bosc-2 (Fig. 8), for which there is again no significant change in mass or volume between uncrenulated and crenulated domains. These plots compare averages over larger volumes, but a comparison of the weight % of the major components normalized against Al_2O_3 for the six samples around Bosc-1 also shows very little variation between samples (Fig. 9). The consistency between Bosc-1A and B (both from the region of planar earlier foliation, Fig. 1) confirms that the initial composition prior to crenulation was effectively homogeneous.

The X-ray powder diffraction patterns of Fig. 10

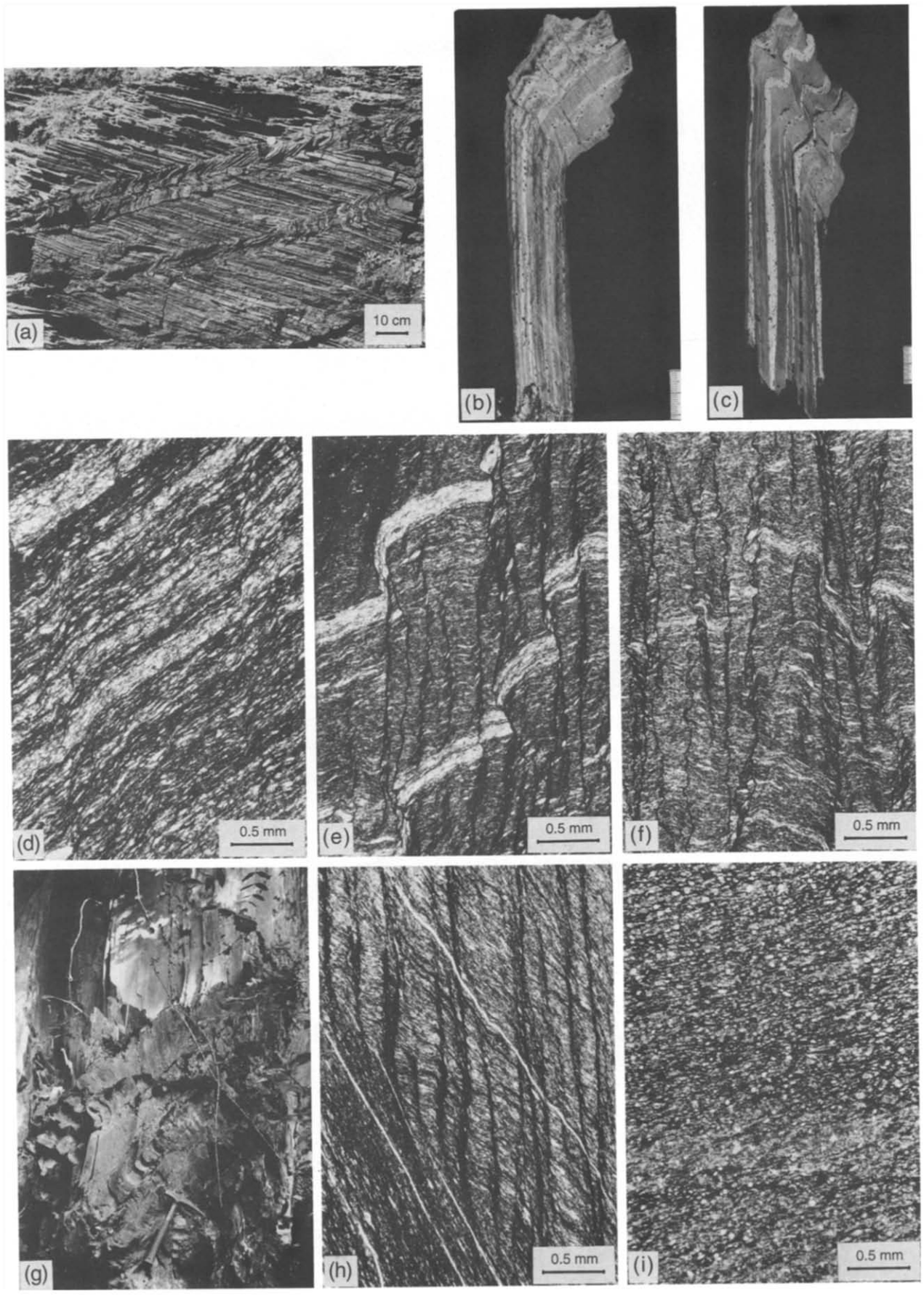

Fig. 5. (a) Typical banded appearance of 'zigzag folds' in dark phyllites from Penally Point, Boscastle, SW England (cf. Dearman & Freshney 1966, fig. 2). A new crenulation cleavage develops as axial plane to folds within the band. (b) Photograph of sample Bosc-1 (cf. Fig. 1). (c) Photograph of sample Bosc-2 (cf. Fig. 2). (d) Photomicrograph of sample Bosc-1A from the very weakly crenulated region of planar pre-existing cleavage. (e) Photomicrograph of sample Bosc-1C from the transition into the crenulated zone. (f) Photomicrograph of sample Bosc-1D from the crenulated zone. (g) Overview of the quarry outcrop 2 km southeast of Bernkastel, Moselle Valley, Germany, from which Hun-1 and Hun-2 were collected. Note the predominantly planar steep slaty cleavage and the cross-cutting bands of folding and new crenulation cleavage. (h) Photomicrograph of sample Hun-2B from the limb of the crenulation fold. (i) Photomicrograph of sample Hun-2E from the hinge of the crenulation fold.

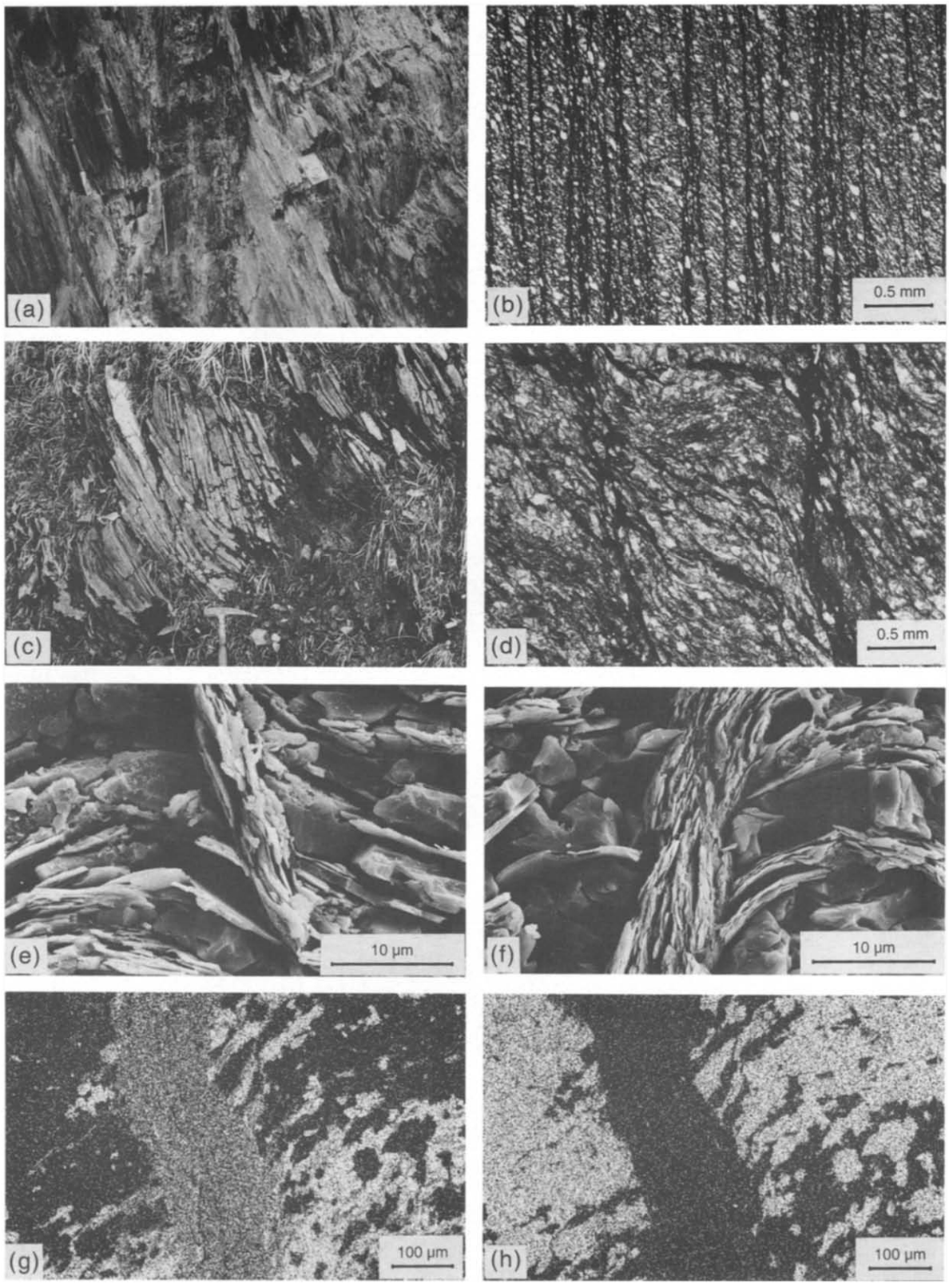

Fig. 6. (a) Outcrop of Hunsrückschiefer slates on the left bank of the Moselle River, opposite Leiwen, Germany. Note the band of strongly developed steep crenulation cleavage (from which sample Hun-4 was collected) within the more weakly overprinted slates (sample Hun-3). (b) Photomicrograph of the strongly crenulated sample Hun-4. (c) View looking northeast of the outcrop at the northeastern end of Lac de Roselend, near Beaufort, French Alps (see sketch, Fig. 4). (d) Photomicrograph of the overprinting crenulation cleavage developed in sample Ros-2. (e) Scanning electron photomicrograph of a single crenulation cleavage domain in sample Bosc-1. Note the relatively discrete nature of the cleavage domain and the strong mineralogical differentiation, with quartz and albite practically absent from the cleavage domain. (f) Scanning electron photomicrograph of discrete crenulation cleavage developed in sample Ros-5. Note the strong mineralogical differentiation, with calcite practically absent from the cleavage domain, (g) Si X-ray map for a crenulation cleavage domain in sample Ros-5. (h) Ca X-ray map of the same crenulation cleavage domain. Note the strong depletion of Ca in the cleavage domain.

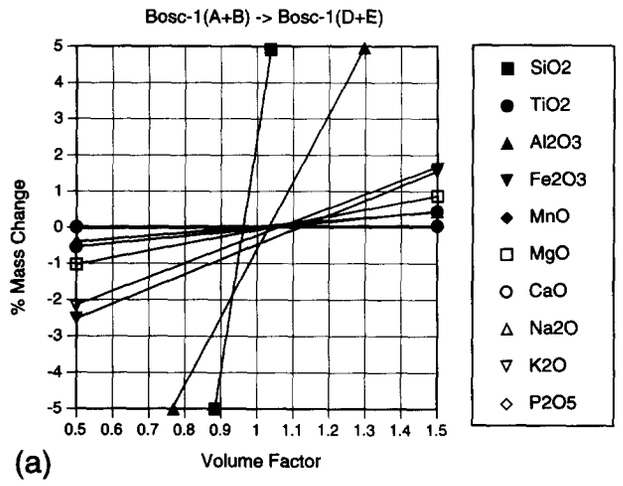

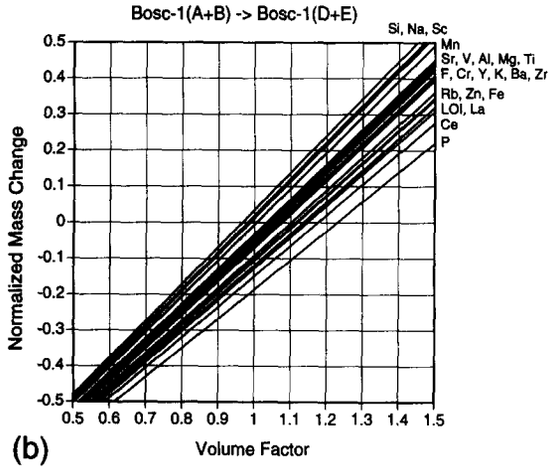

Fig. 7. (a) Standard Gresens plot comparing the major element chemistry of the planar-foliated region of Bosc-1 (average of A+B) with the more strongly crenulated region (average of D+E). (b) Normalized Gresens plot for the same samples.

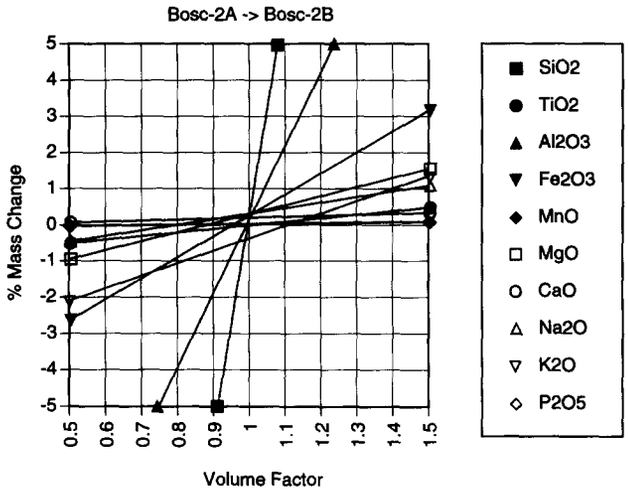

Fig. 8. Standard Gresens plot comparing the major element chemistry of the planar-foliated region of Bosc-2 (A) with the more strongly crenulated region (B).

demonstrate that there is no mineralogical difference between the six samples from Bosc-1; they all consist of quartz, muscovite, chlorite and albite. Since there is no significant difference in chemistry, volume or mineralogy, the calculated mineral mode of the samples also cannot vary (43% quartz, 35% muscovite, 14% chlorite, 8% albite, by volume), which is also qualitatively implied by the similar diffraction peak heights in Fig. 10. However, on the smaller scale of individual cleavage and microlithon domains, there is clearly a dramatic mineralogical and chemical differentiation (see Fig. 6e). This implies that the local redistribution of mass and volume must occur on a length-scale smaller than the cm-scale of the chemically analysed samples.

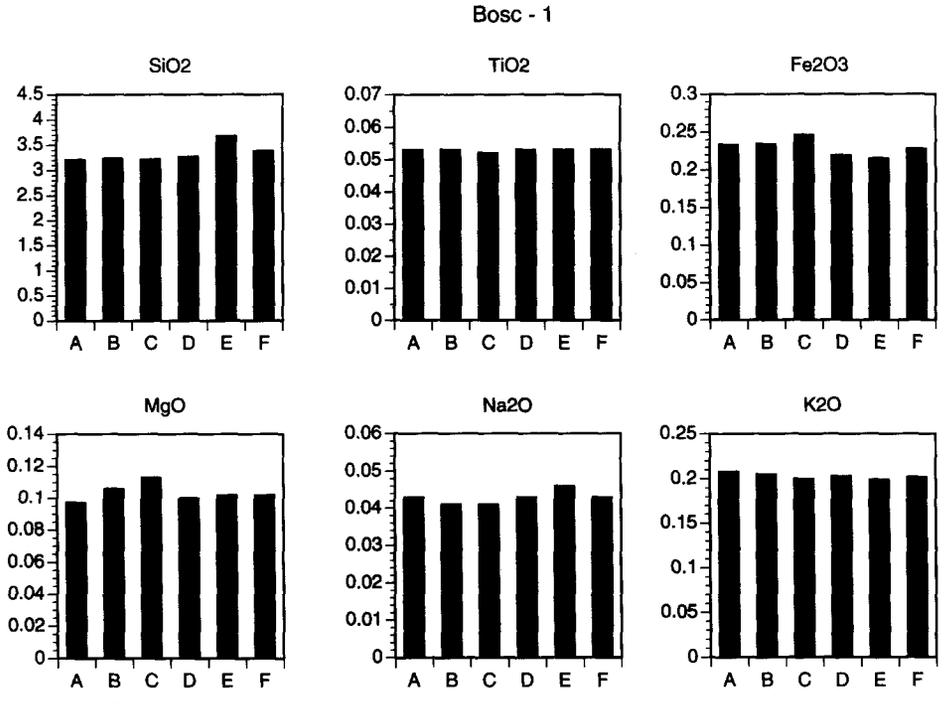

Fig. 9. Weight % of major elements, normalized against weight % Al_2O_3, for samples Bosc-1A–F.

Moselle Valley

Very similar results to those from Boscastle are obtained from a comparison between samples Hun-1 and Hun-2 from the Moselle Valley (Fig. 11). Overall, there is very little volume change between the crenulated and uncrenulated domains, with perhaps a slight relative volume increase (< 5%) within the crenulated domains. However, in these samples the wavelength of folding of the earlier foliation is sufficiently large that a comparison can be made for samples at different positions around a single fold (Hun-2, Fig. 3b). The weight % ratios relative to Al_2O_3 show a consistent pattern to the compositional variation in major elements around the fold (Fig. 12): SiO_2, Na_2O, total Fe (as Fe_2O_3) and MgO are depleted and K_2O enriched in the limb regions (Hun-2A, B and F), where cleavage domains are common, relative to the hinge region (Hun-2C, D and E), where cleavage domains are rare. If Al_2O_3 and TiO_2 are assumed to be immobile (as suggested by the constancy of the TiO_2/Al_2O_3 ratio in Fig. 12), then the normalized Gresens plots of Fig. 13 show that there has been a ~45% volume loss in Hun-2A on the limb of the fold and a ~30% volume gain in Hun-2D in the hinge of the fold relative to the unfolded region of Hun-1. However, weighting each sample for its width perpendicular to the crenulation cleavage produces an average composition for the whole fold (i.e. between the inflection points) which does not differ significantly in volume or mass from the uncrenulated material (Fig. 11). The variation in chemical composition between the unfolded region and the limb and hinge of the fold is also reflected in the calculated mineral modes: Hun-1 has an average mode of 54% quartz, 22% chlorite, 15% muscovite and 9% albite, whereas Hun-2A has 21% quartz, 33% chlorite, 39% muscovite and 7% albite and Hun-2-D 62% quartz, 17% chlorite, 10% muscovite and 11% albite. The relative depletion of Fe in the fold limb region relative to both the hinge region and the unfolded region is seen in the muscovite to chlorite ratio: Hun-1 has an average ratio of 0.7, Hun-2A 1.2 and Hun-2D 0.6. Comparing Fig. 13(a) & (b) indicates that some minor elements are consistently redistributed between limb and hinge, with an increase in Rb, Ba, Y and Sc, and a decrease in F, P_2O_5 and CaO in the limb relative to the hinge.

The second locality from the Moselle Valley considers a band of strongly developed crenulation cleavage (sample Hun-4) bounded to either side by much more weakly crenulated material (sample Hun-3, Fig. 6a). There is no clear mesoscopic folding of the earlier foliation (Fig. 6a). Assuming immobility of Al_2O_3 and TiO_2, the normalized Gresens plot of Fig. 14 indicates a significant relative volume loss from the crenulated zone, on the order of 35–40%. This is associated with the loss of SiO_2, Na_2O, P_2O_5, CaO, MgO, total Fe (as Fe_2O_3) and F, and gains of K_2O, Rb, Y, Ce, Sc and Ba in the crenulated zone. The calculated mineral mode for the weakly crenulated sample Hun-3 is 56% quartz, 18% muscovite, 15% chlorite and 11% albite (muscovite to chlorite ratio 1.1) whereas for the strongly crenulated

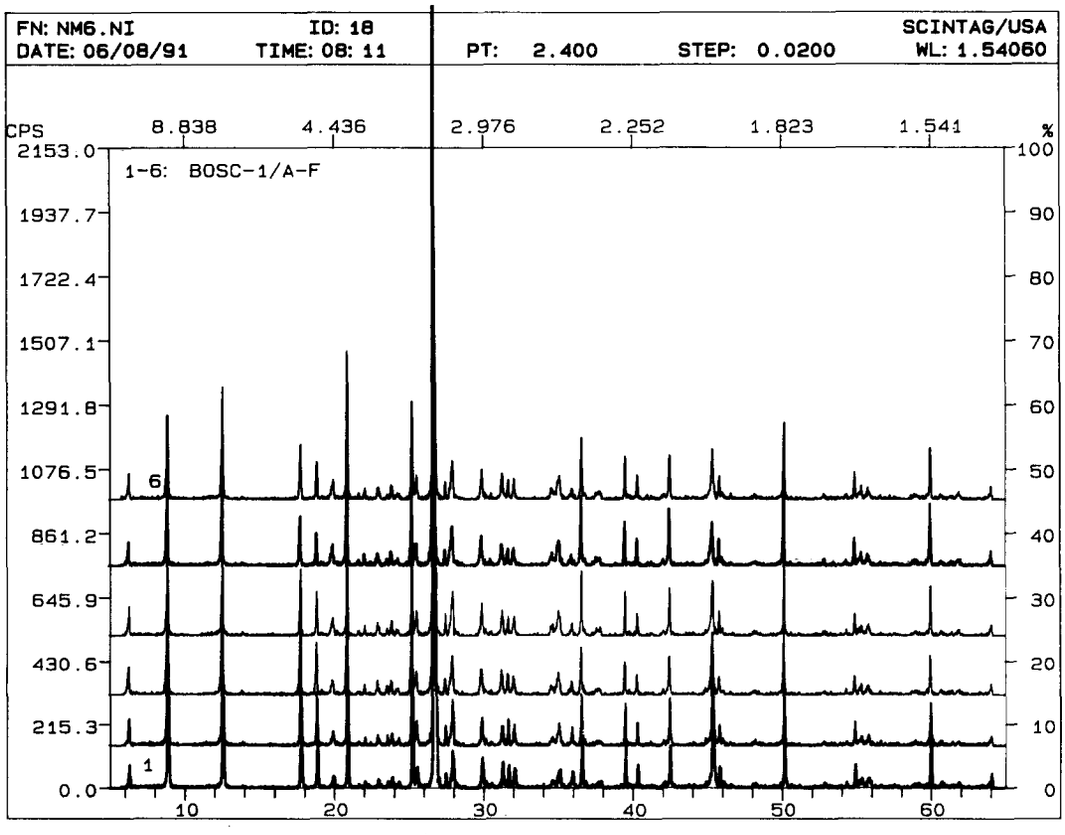

Fig. 10. X-ray powder diffraction patterns for Bosc-1A–F (traces 1–6, respectively). Minerals present in significant quantities are quartz, chlorite, muscovite and albite.

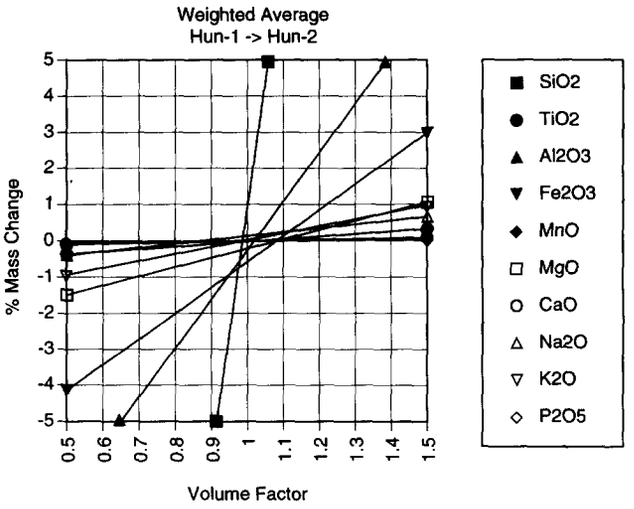

Fig. 11. Standard Gresens plot comparing the major element chemistry of the averaged bulk composition of Hun-1 and Hun-2. Averages are weighted for the width of each sample perpendicular to the crenulation cleavage.

sample Hun-4 it is 33% quartz, 33% muscovite, 23% chlorite and 11% albite (muscovite to chlorite ratio 1.5). These results are very similar to those observed between the weakly crenulated region and the fold limb region of samples Hun-1 and Hun-2A. The geometry is also not dissimilar, as in both cases the orientation of the earlier foliation in the microlithons is little different from that in the weakly crenulated region, but there is a greater development of cleavage domains. It seems likely that the mechanisms are also similar for the two localities—at the first locality volume and mass have been redistributed on the hand-specimen scale between limb and hinge regions of the fold, whereas at the second locality the redistribution has occurred on a scale larger than the outcrop itself and there has been an overall volume loss from the band of strong crenulation cleavage.

Lac de Roselend

The samples from Lac de Roselend were collected to compare the behaviour of calcite-rich crenulated rocks with the calcite-absent samples from Boscastle and the Moselle Valley. Unfortunately, the initial composition of these rocks is not as homogeneous as the finer-grained slates from the other localities and this introduces some additional variability. Despite this natural limitation, the Gresens plot of Fig. 15 again demonstrates that if anything there is a relative increase in volume within the strongly crenulated regions, largely due to an increase in calcite content ($CaO + CO_2$). On the sample scale (*ca* 1 kg samples), the chemical variation is still small (Fig. 16) when compared with the variation that occurs between individual cleavage domains and microlithons (Figs. 6g & h). Individual cleavage domains are practically calcite-free (Fig. 6f) and are consequently strongly depleted in Ca (Fig. 6h) and enriched in Al, K, Fe and Ti compared to the microlithons (Fig. 17).

DISCUSSION

The results from the different localities are very consistent. On the scale of individual crenulation microfolds, there is a loss of volume from the cleavage domains which is generally balanced by a corresponding volume gain in the adjacent microlithons such that volume is effectively conserved on the scale of cm-sized samples (e.g. Bosc-1). If larger scale crenulation folds in the pre-existing foliation are developed with an associ-

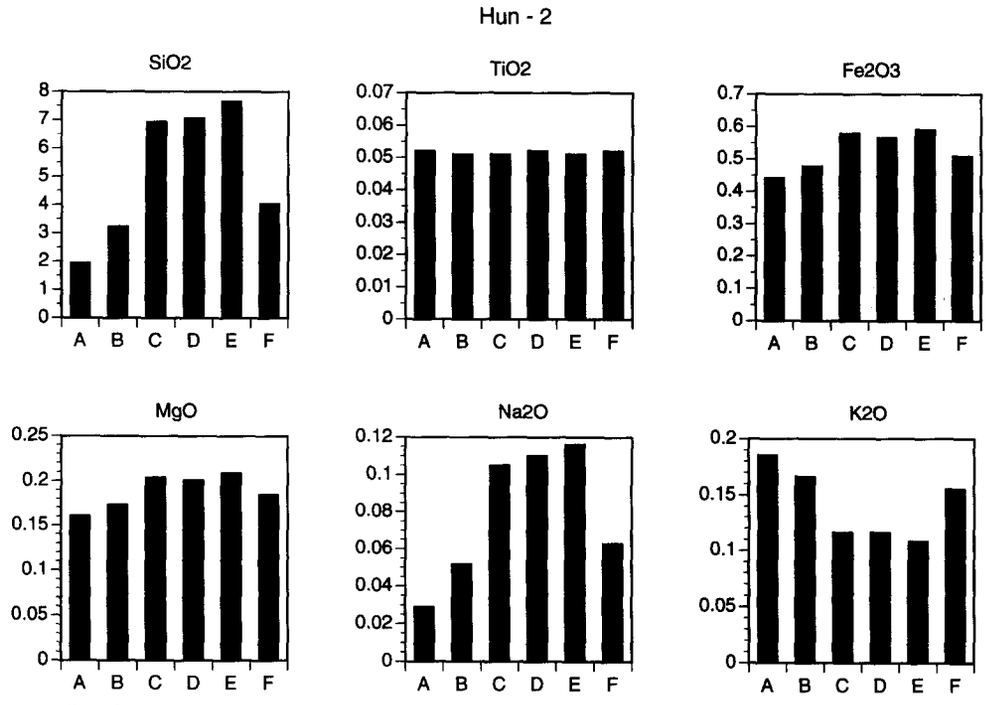

Fig. 12. Weight % of major elements, normalized against weight % Al_2O_3, for samples Hun-2A–F.

ated concentration of cleavage domains in the limb regions relative to the hinges, then volume redistribution will occur on the scale of the fold wavelength (e.g. Hun-2). In general, there is a mass loss of SiO_2, CaO, CO_2, Na_2O, P_2O_5, MgO, total Fe (as Fe_2O_3) and F, and gains of K_2O, Rb, Y, Ce, Sc and Ba in the cleavage domains, with the opposite observed for the microlithons. The consistent mass loss in total Fe from the strongly cleaved domains (e.g. Fig. 13) was also noted by Marlow & Etheridge (1977) and in their examples corresponded to an increase in the muscovite to biotite ratio in cleavage domains. In the lower metamorphic grade samples considered here, a comparable increase in the ratio of muscovite to chlorite ratio occurs in the cleavage domains, a redistribution also noted by Cosgrove (1976).

With the exception of the second Moselle Valley locality (samples Hun-3 and -4), all samples show a tendency for a slight *relative* increase in volume within the strongly crenulated regions compared to the uncrenulated regions, on a scale larger than the wavelength of individual crenulation folds. However, the 'uncrenulated' samples themselves often show occasional isolated cleavage domains (e.g. Fig. 5d) and these narrow domains are clearly associated with a local volume loss. The samples taken to represent the initial uncrenulated bulk composition may therefore actually have undergone a minor volume loss, with this material either transferred to the strongly crenulated region or lost from the system on the scale considered.

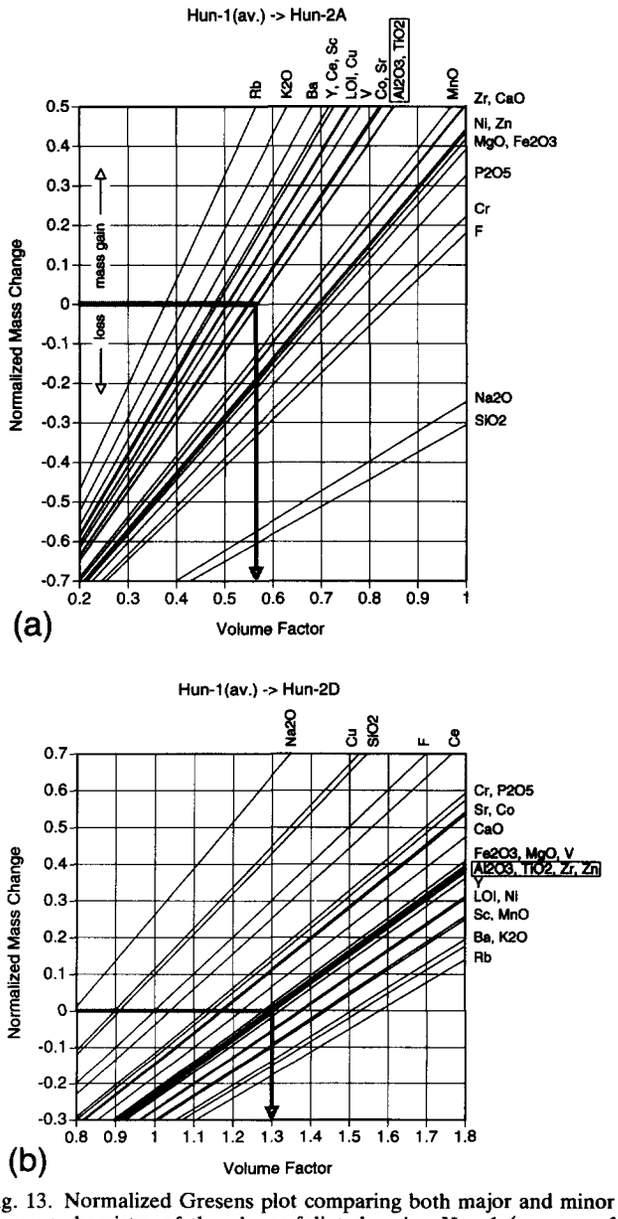

Fig. 13. Normalized Gresens plot comparing both major and minor element chemistry of the planar foliated region Hun-1 (average of A+B+D) with (a) the strongly crenulated limb region of Hun-2A and (b) the hinge region of Hun-2D.

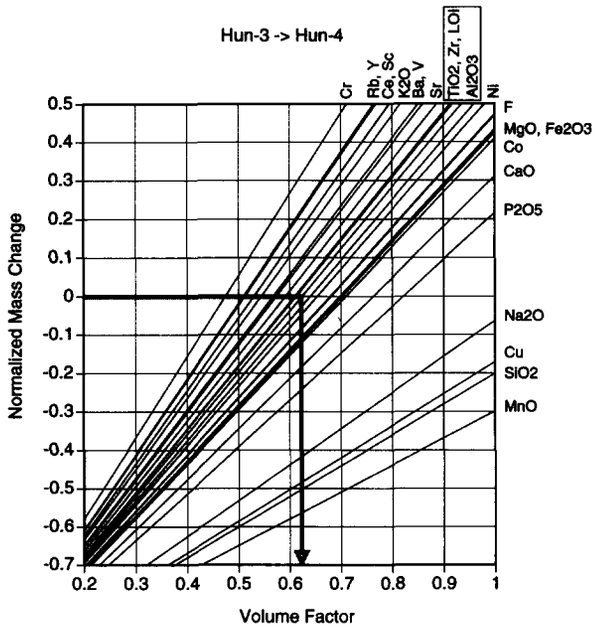

Fig. 14. Normalized Gresens plot comparing both major and minor element chemistry of Hun-3 from the weakly crenulated region with Hun-4 in the band of strongly developed crenulation cleavage.

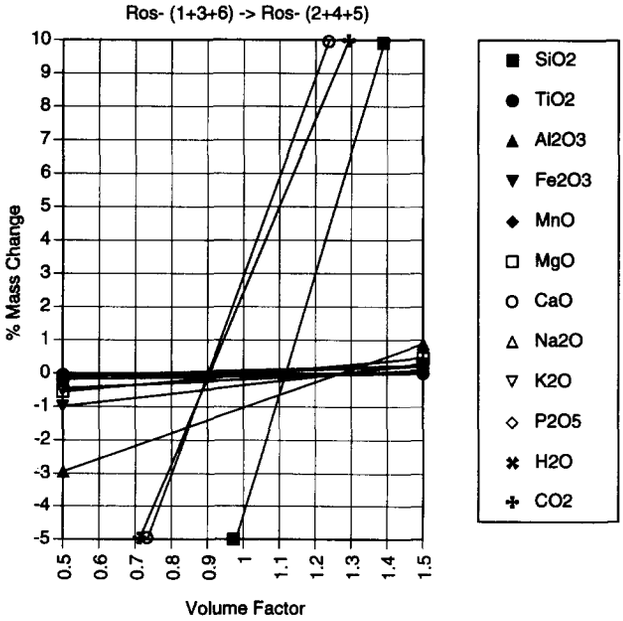

Fig. 15. Standard Gresens plot comparing the major element chemistry of the averaged bulk composition of weakly crenulated regions (Ros-1+3+6) with strongly crenulated regions (Ros-2+4+5).

For all the examples considered here, the outcrop-scale geometry could be described in terms of a series of asymmetric 'folds', with one long, straight, weakly-crenulated limb and one short limb with a more strongly developed crenulation cleavage (Figs. 1–4, 5a and 18a). These mesoscopic folds are not, however, simply higher order crenulation folds, even if there may be minor volume transfer from limb to hinge, as discussed above. Folds from the crenulated zone always show a strong concentration of crenulation cleavage domains in the fold limbs relative to the hinge, which is the exact opposite of the geometry of the outcrop-scale asymmetric folds, where cleavage development is concentrated in the hinge and is very weak on the limbs.

The isolated zones of crenulation cleavage from Boscastle and the Moselle Valley occur as narrow bands of meso- and microfolding, which make an angle <45° to the pre-existing well-developed foliation (e.g. Fig. 18a). As extensively discussed by Ramsay & Graham (1970), Cobbold (1977a,b) and Ramsay (1980), the geometry of a long narrow parallel-sided band constrains the heterogeneous strain component to be some combination of volume loss or gain (related to a change in width of the zone) and simple shear parallel to the band boundary. This heterogeneous component may be superimposed on a homogeneous background strain affecting both the band and its surroundings. The present study has shown that the volume change involved in the development of several classical examples of isolated narrow zones of crenulation cleavage from Boscastle and the Moselle Valley is insignificant: the additional heterogeneous strain within these parallel-sided band-like zones must therefore be related to a component of heterogeneous simple shear parallel to the band boundaries. The banded structures represent isolated shear zones developed in already strongly foliated material. In the cases considered, the shear sense was such that the pre-existing foliation was progressively shortened and buckled (Fig. 18b), often leading to several orders of folding ranging from microfolds in the foliation (the crenulations, with cleavage domains developed on the limbs) to larger scale folds determined by the lithological layering (Fig. 18a). Volume and mass is redistributed on the scale of this folding, whether these be microfolds or larger scale folds, with volume lost from the limbs and gained in the hinges (Fig. 13).

The crenulation cleavage developed in the isolated bands has an average orientation parallel to the band boundaries (Fig. 18a) and thus parallel to the shear plane of the heterogeneous simple shear component. The cleavage planes cannot, therefore, be strictly parallel to the XY principal plane of the finite strain ellipsoid (with principal axes $X>Y>Z$, cf. Fig. 18b). As discussed by Williams (1976), domainal cleavages linked to material points, such as crenulation cleavage, cannot track the XY plane in a rotational deformation, and precise parallelism with the principal plane should not generally be expected (see also Hoeppener 1956, Talbot 1964, Hobbs *et al.* 1976, Williams 1976, Ghosh 1982). Approximate parallelism, as reported from natural examples by Gray & Durney (1979), may still be achieved if the additional homogeneous component is large compared to the heterogeneous simple shear component. However, the isolated zones of crenulation cleavage from the Moselle Valley, for example, are volumetrically very subordinate to the predominant regional planar slaty cleavage (e.g. Talbot 1964). It would seem more reasonable to relate the development

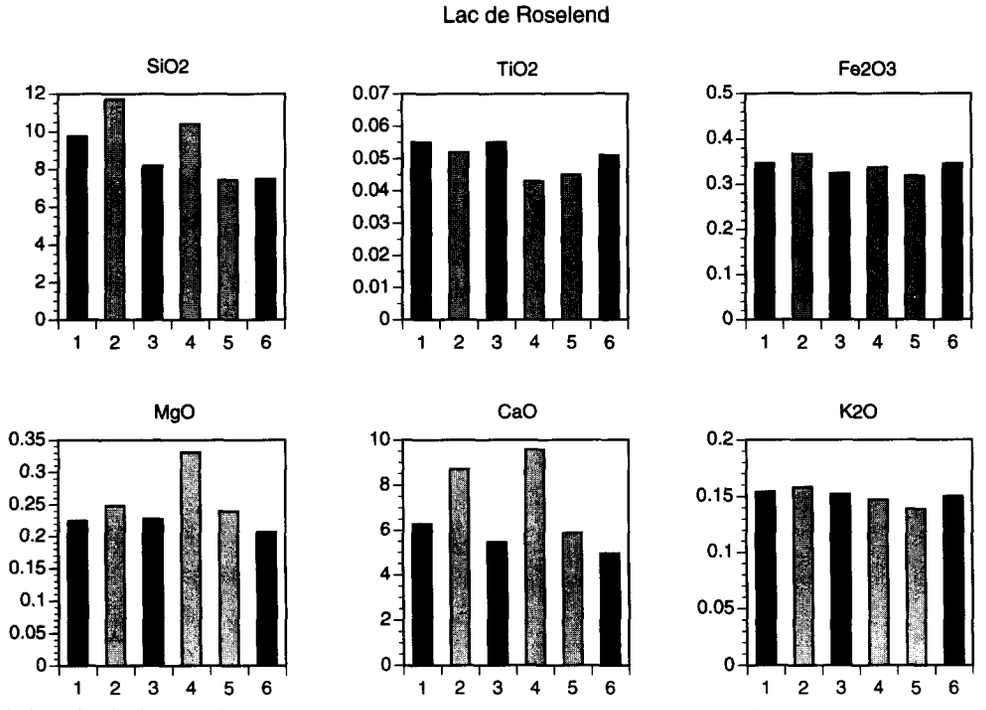

Fig. 16. Weight % of major elements, normalized against weight % Al_2O_3, for samples Ros-1–6. Solid bars correspond to weakly crenulated regions, open formed bars to strongly crenulated regions.

of these small local zones to strain heterogeneities of correspondingly local significance rather than to invoke an all-pervasive, regional high-strain event.

Unfortunately, the magnitude of the heterogeneous shear strain component in the crenulation zones cannot be accurately quantified unless the background homogeneous strain component is also known. In Fig. 18(b), the trace of the lithological layering in Fig. 18(a) has been used to estimate the shear strain component at around $\gamma = 2$ for the case in which the width of the band has not changed during deformation. This implies that *both* the homogeneous strain component and the volume change are negligible—only the volume change has actually been demonstrated to be negligible in the present study. The geometry of Fig. 18(b) therefore represents only one end-member of the range of possible geometries; as noted above, the other end-member corresponds to the case where the homogeneous component completely dominates.

The crenulated domains observed in the Lac de Roselend area have a distinctly different geometry and probably represent intrafolial fold packets developed during continued shear when the dominant foliation is locally deflected through the shear plane, and thus into an orientation where it is progressively shortened and rotated (e.g. Tricart 1980). Within these packets, volume is locally redistributed between fold limbs and hinges on a range of scales, but without evidence of significant overall modification of mass or volume for the packet as a whole (e.g. Fig. 15).

CONCLUSIONS

Isolated bands of crenulation cleavage can develop without significant overall volume change or mass transport. This is established very clearly for the samples from Boscastle and in samples Hun-1 and Hun-2 from the Moselle Valley. Volume loss on a scale larger than the individual microlithon and cleavage domains is not, therefore, a prerequisite for the development of crenulation cleavage, although it can also occur. At one location in the Moselle Valley (samples Hun-3 and -4), volume loss on the order of 35–40% occurs by removal

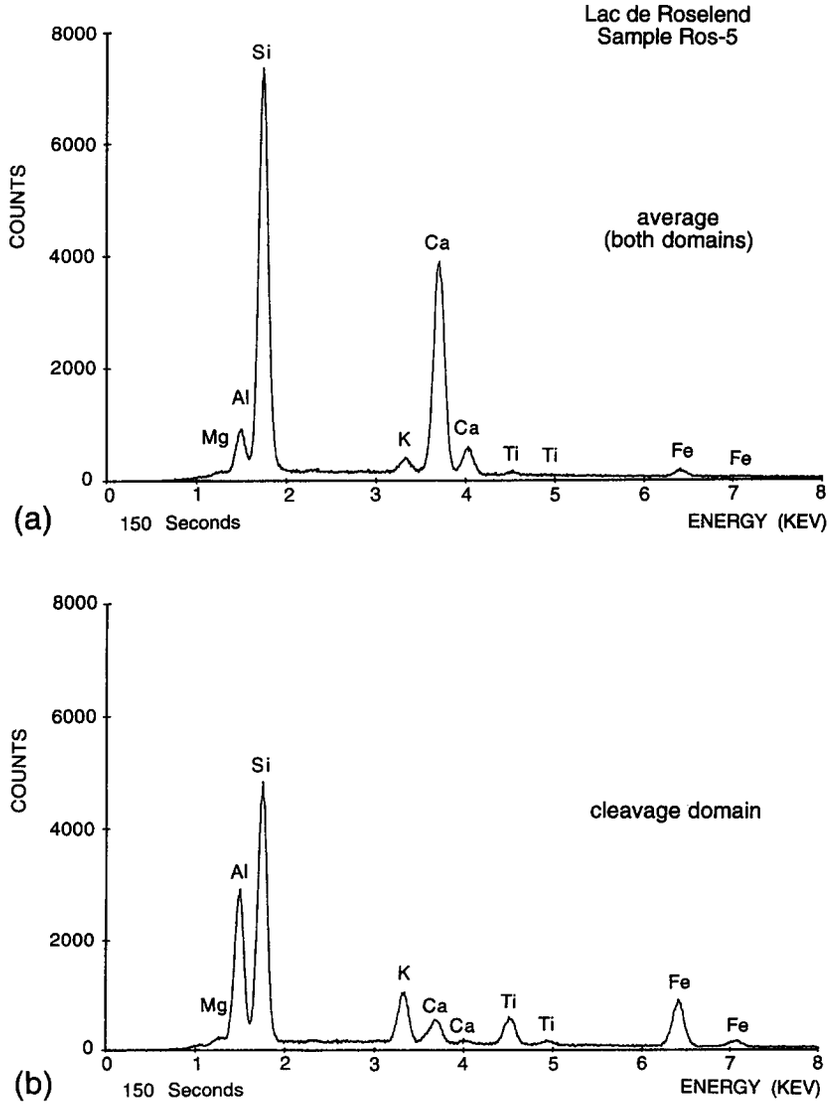

Fig. 17. X-ray fluorescence counts (a) averaged over the whole of Fig. 6(g) (both cleavage and microlithon domains) and (b) from the cleavage domain alone (centre of Fig. 6g) for sample Ros-5.

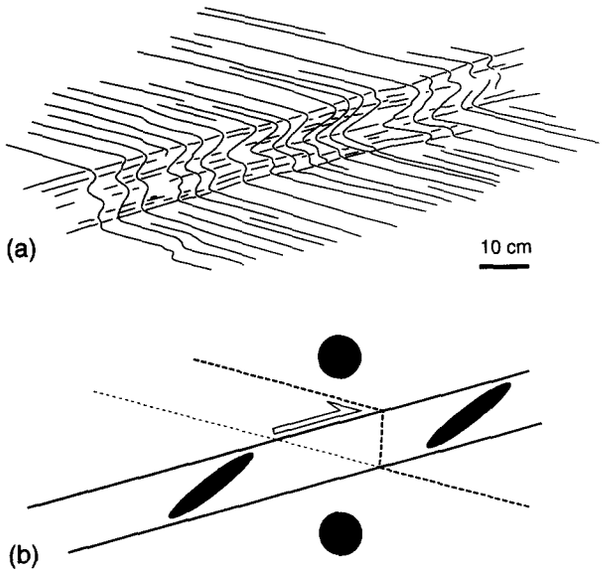

Fig. 18. (a) Sketch of the zone of 'zigzag' folding and axial planar crenulation cleavage in the upper part of Fig. 5(a) from Penally Point, Boscastle, SW England. Note that the zone is effectively parallel-sided and long relative to its width, typical of the band-like structures discussed by Ramsay & Graham (1970), Cobbold (1977a,b) and Ramsay (1980). Note also that the crenulation cleavage is effectively parallel to the band boundaries. Individual layers can be followed from one side, through the crenulated zone, to the other side (cf. Fig. 5a). (b) Interpretation of the heterogeneous strain component inside the band of crenulation cleavage in terms of a simple shear zone, with $\gamma \approx 2$. Note that this geometry only represents one possible end-member, when the background homogeneous strain is negligible compared to the heterogeneous strain component.

of the most soluble component, namely SiO_2 (as quartz). Regardless of their mechanical significance, the narrow parallel-sided bands of crenulation cleavage from Boscastle and the Moselle Valley have the geometry of isolated shear zones developed in anisotropic, foliated rocks and like shear zones developed in more isotropic rocks (e.g. granitoids, Ramsay 1980) can develop both with or without volume change or metasomatism (e.g. Simpson 1981, Marquer *et al.* 1985). If the range of samples analysed in this study are representative and, despite their limited numbers, they do come from various 'classic' localities for the description of crenulation cleavage, then significant volume change during crenulation cleavage development may be more the exception than the rule, and is not critical for the formation of this common domainal cleavage type.

Acknowledgements—This research was supported by research grant 0-15-908-90 from the ETH-Zürich. Thanks to John Ramsay and Sara Spencer, who introduced me to the Boscastle and Lac de Roselend areas, respectively; to Stefan Hesske, who prepared the samples for XRF analysis and measured the sample densities with the pycnometer; to Djordje Grujic for the SEM studies; and to Noldi Stahel for help with the X-ray powder diffraction measurements. John Cosgrove and David Gray are thanked for their thorough reviews of the manuscript.

REFERENCES

Bell, T. H. & Cuff, C. 1989. Dissolution, solution transfer, diffusion versus fluid flow and volume loss during deformation/metamorphism. *J. metamorph. Geol.* **7**, 425–448.

Borradaile, G. J., Bayly, M. B. & Powell, C. M. 1982. *Atlas of Deformational and Metamorphic Rock Fabrics*. Springer, Berlin.

Carmichael, D. M. 1969. On the mechanism of prograde metamorphic reactions in quartz-bearing pelitic rocks. *Contr. Miner. Petrol.* **20**, 244–267.

Cobbold, P. R. 1977a. Description and origin of banded deformation structures. I. Regional strain, local perturbations, and deformation bands. *Can. J. Earth Sci.* **14**, 1721–1731.

Cobbold, P. R. 1977b. Description and origin of banded deformation structures. II. Rheology and the growth of banded perturbations. *Can. J. Earth Sci.* **14**, 2510–2523.

Cosgrove, J. W. 1976. The formation of crenulation cleavage. *J. geol. Soc. Lond.* **132**, 155–178.

Dearman, W. R. & Freshney, E. C. 1966. Repeated folding at Boscastle, North Cornwall, England. *Proc. Geol. Ass.* **77**, 199–215.

Ghosh, S. K. 1982. The problem of shearing along axial plane foliations. *J. Struct. Geol.* **4**, 63–67.

Gray, D. R. 1977a. Differentiation associated with discrete crenulation cleavages. *Lithos* **10**, 89–101.

Gray, D. R. 1977b. Morphologic classification of crenulation cleavage. *J. Geol.* **85**, 229–235.

Gray, D. R. 1979. Geometry of crenulation-folds and their relationship to crenulation cleavage. *J. Struct. Geol.* **1**, 187–205.

Gray, D. R. 1987. Crenulation cleavages. In: *The Encyclopedia of Structural Geology and Plate Tectonics* (edited by Seyfert, C. K.). Van Nostrand Reinhold, New York, 158–165.

Gray, D. R. & Durney, D. W. 1979. Investigations on the mechanical significance of crenulation cleavage. *Tectonophysics* **58**, 35–79.

Gresens, R. L. 1967. Composition–volume relationships of metamorphism. *Chem. Geol.* **2**, 47–65.

Hobbs, B. E., Means, W. D. & Williams, P. F. 1976. *An Outline of Structural Geology*. John Wiley, New York.

Hoeppener, R. 1956. Zum Problem der Bruchbildung, Schieferung und Faltung. *Geol. Rdsch.* **45**, 247–283.

Hutchinson, C. S. 1975. *Laboratory Handbook of Petrographic Techniques*. John Wiley, New York.

Klein, H. H. 1976. Alumosilikatführende Knauern im Lepontin. *Schweiz. miner. petrogr. Mitt.* **56**, 435–456.

Knill, J. L. 1960. A classification of cleavages, with special reference to the Graignish District of the Scottish Highlands. *Int. Geol. Congress Reps 21st Session, Part* 18, 317–325.

Leith, C. K. 1905. Rock cleavage. *Bull. U.S. geol. Surv.* **329**.

Mancktelow, N. S. 1982. A boundary model for the development of crenulations and crenulation cleavage. *Mitt. Geol. Inst. ETH & Univ. Zürich, N.F.* **239a**, 182–185.

Marlow, P. C. & Etheridge, M. A. 1977. Development of a layered crenulation cleavage in mica schists of the Kanmantoo Group near Macclesfield, South Australia. *Bull. geol. Soc. Am.* **88**, 873–882.

Marquer, D., Gapais, D. & Capdevila, R. 1985. Comportement chimique et orthogneissification d'une granodiorite en facies schistes verts (Massif de l'Aar, Alpes centrales). *Bull. Mineral.* **108**, 209–221.

Mills, K. J. 1964. The structural petrology of an area east of Springton, South Australia. Unpublished Ph.D. thesis, University of Adelaide.

Nicholson, R. 1966. Metamorphic differentiation in crenulated schists. *Nature* **209**, 68–69.

Potdevin, J. L. & Marquer, D. 1987. Méthodes de quantification des transferts de matière par les fluides dans les roches métamorphiques déformées. *Geodin. Acta* **1**, 193–206.

Ramsay, J. G. 1980. Shear zone geometry: a review. *J. Struct. Geol.* **2**, 83–99.

Ramsay, J. G. & Graham, R. H. 1970. Strain variation in shear belts. *Can. J. Earth Sci.* **7**, 786–813.

Rickard, M. J. 1961. A note on cleavage in crenulated rocks. *Geol. Mag.* **98**, 324–332.

Simpson, C. 1981. Ductile shear zones: a mechanism of rock deformation in the orthogneiss of the Maggia Nappe, Ticino. Unpublished Ph.D. thesis, ETH Zürich.

Spencer, S. 1989. The Nature of the North Pennine Front: French Alps. Unpublished Ph.D. thesis, Imperial College, London.

Talbot, J. L. 1964. Crenulation cleavage in the Hunsrückschiefer of the Middle Moselle region. *Geol. Rdsch.* **26**, 1026–1043.

Talbot, J. L. & Hobbs, B. E. 1968. The relationship of metamorphic differentiation to other structural features at three localities. *J. Geol.* **76**, 581–587.

Tricart, P. 1980. Tectoniques superposées dans les Alpes occidentales, au sud du Pelvoux. Evolution structurale d'une chaine de collision. Unpublished thèse d'état, Strasbourg.

Van den Driessche, J. & Brun, J.-P. 1987. Rolling structures at large shear strain. *J. Struct. Geol.* **9**, 691–704.

Weber, K. 1981. Kinematic and metamorphic aspects of cleavage

formation in very low-grade metamorphic slates. *Tectonophysics* **78**, 291–306.

Williams, P. F. 1972. Development of metamorphic layering and cleavage in low-grade metamorphic rocks at Bermagui, Australia. *Am. J. Sci.* **272**, 1–47.

Williams, P. F. 1976. Relationship between axial-plane foliations and strain. *Tectonophysics* **30**, 181–196.

Williams, V. A. 1982. Differentiated crenulation cleavage. In: *Atlas of Deformational and Metamorphic Rock Fabrics* (edited by Borradaile, G. J., Bayly, M. B. & Powell, C. M.). Springer, Berlin, 92–93.

APPENDIX

Table A1. XRF whole-rock analyses

	Bosc-1A	Bosc-1B	Bosc-1C	Bosc-1D	Bosc-1E	Bosc-1F	Bosc-1(A+B)	Bosc-1(D+E)	Bosc-2A	Bosc-2B
Weight %										
SiO_2	61.40	61.87	61.55	62.48	65.76	63.10	61.64	64.12	59.57	58.92
TiO_2	1.02	1.02	1.00	1.01	0.95	0.99	1.02	0.98	1.02	0.99
Al_2O_3	19.16	19.13	19.14	19.14	17.87	18.66	19.15	18.51	20.32	20.15
Fe_2O_3	4.47	4.47	4.71	4.19	3.85	4.25	4.47	4.02	5.58	5.75
MnO	0.06	0.06	0.07	0.06	0.06	0.06	0.06	0.06	0.10	0.13
MgO	1.85	2.03	2.16	1.92	1.83	1.90	1.94	1.88	2.22	2.48
CaO	0.01	0.00	0.01	0.02	0.04	0.03	0.01	0.03	0.07	0.27
Na_2O	0.82	0.79	0.78	0.83	0.82	0.80	0.81	0.83	1.24	1.53
K_2O	3.98	3.92	3.82	3.89	3.56	3.76	3.95	3.73	3.85	3.42
P_2O_5	0.06	0.05	0.04	0.05	0.04	0.06	0.06	0.05	0.08	0.11
Ignition loss	5.08	4.77	4.82	4.67	4.05	4.89	4.93	4.36	6.49	5.19
Total	97.91	98.11	98.10	98.26	98.83	98.50	98.01	98.55	100.54	98.94
ppm										
F	675	602	650	603	621	789	638.5	612.0	656	473
Ba	546	539	527	534	488	513	542.5	511.0	533	387
Rb	178	177	168	170	154	165	177.5	162.0	171	133
Sr	55	54	51	54	52	54	54.5	53.0	73	95
La	56	58	55	55	45	49	57.0	50.0	45	21
Ce	73	79	79	72	58	77	76.0	65.0	61	43
Y	23	20	22	21	20	20	21.5	20.5	27	24
Zr	209	194	191	194	183	199	201.5	188.5	193	171
V	196	197	193	197	183	188	196.5	190.0	211	151
Cr	217	221	208	211	208	214	219.0	209.5	157	131
Ni	5	4	5	5	4	4	4.5	4.5	7	15
Co	28	15	12	13	11	10	21.5	12.0	13	9
Cu	11	8	7	12	14	18	9.5	13.0	17	12
Zn	55	57	57	56	45	48	56.0	50.5	64	66
Sc	28	27	27	29	27	29	27.5	28.0	30	24

	Hun-1A	Hun-1B	Hun-1C	Hun-1D	Hun-2A	Hun-2B	Hun-2C	Hun-2D	Hun-2E	Hun-2F	Hun-1av	Hun-2av	Hun-3	Hun-4
Weight %														
SiO_2	66.05	67.60	71.09	68.10	46.36	58.96	74.30	74.80	75.93	63.97	67.63	68.21	71.43	56.92
TiO_2	0.76	0.71	0.61	0.71	1.25	0.93	0.55	0.55	0.51	0.83	0.72	0.69	0.61	1.00
Al_2O_3	14.39	13.50	12.22	13.51	23.90	18.20	10.71	10.59	9.93	15.82	13.66	13.31	13.34	20.79
Fe_2O_3	7.61	7.75	7.07	7.77	10.53	8.69	6.20	5.99	5.86	8.06	7.62	7.00	5.54	7.79
MnO	0.07	0.07	0.06	0.08	0.11	0.08	0.06	0.05	0.05	0.08	0.07	0.07	0.10	0.07
MgO	2.72	2.79	2.52	2.81	3.85	3.15	2.18	2.13	2.08	2.93	2.74	2.51	1.86	2.66
CaO	0.21	0.19	0.17	0.19	0.29	0.26	0.16	0.16	0.15	0.22	0.19	0.19	0.13	0.17
Na_2O	0.83	0.91	0.93	1.04	0.69	0.94	1.12	1.17	1.15	0.99	0.92	1.05	1.23	1.15
K_2O	2.12	1.81	1.54	1.77	4.43	3.02	1.24	1.23	1.07	2.46	1.87	1.88	2.16	3.96
P_2O_5	0.19	0.18	0.17	0.18	0.24	0.22	0.16	0.16	0.15	0.20	0.18	0.18	0.14	0.17
Ignition loss	3.38	3.24	2.87	3.18	6.34	4.34	2.42	2.36	2.20	3.55	3.22	3.11	2.62	4.19
Total	98.33	98.75	99.25	99.34	97.99	98.79	99.10	99.19	99.08	99.11	98.83	98.21	99.16	98.87
ppm														
F	560	521	639	609	675	689	535	579	473	693	576	580	511	751
Ba	324	280	239	277	632	447	195	193	168	361	290	283	351	617
Rb	89	74	61	72	203	135	48	49	40	107	77	80	97	190
Sr	39	37	33	37	67	49	34	32	30	43	37	39	51	86
La	27	<20	<20	23	86	46	<20	<20	<20	39	—	—	21	81
Ce	64	59	54	62	125	88	53	59	43	80	61	67	60	113
Y	21	19	17	20	41	26	16	15	14	26	20	20	19	37
Zr	193	189	162	186	278	219	142	143	135	212	186	171	127	207
V	119	110	95	107	210	153	84	86	76	129	110	109	115	200
Cr	220	221	203	221	265	242	192	194	187	223	218	207	193	406
Ni	75	79	71	80	110	88	59	56	56	86	77	69	57	87
Co	19	21	20	20	36	26	17	17	14	27	20	21	19	27
Cu	17	21	17	17	35	46	18	20	37	23	18	28	58	48
Zn	102	103	94	102	144	115	79	78	77	109	101	92	75	110
Sc	18	17	15	17	35	25	12	12	11	21	17	17	17	32

Table A1. (*Continued*)

	Ros-1	Ros-2	Ros-3	Ros-4	Ros-5	Ros-6
Weight %						
SiO_2	41.18	38.65	39.85	33.93	36.28	39.50
TiO_2	0.23	0.17	0.27	0.14	0.22	0.27
Al_2O_3	4.22	3.30	4.87	3.26	4.88	5.27
Fe_2O_3	1.46	1.21	1.58	1.10	1.55	1.82
MnO	0.00	0.00	0.00	0.00	0.01	0.00
MgO	0.95	0.82	1.11	1.08	1.17	1.09
CaO	26.53	28.76	26.54	31.26	28.68	26.12
Na_2O	0.18	0.15	0.13	0.38	0.41	0.44
K_2O	0.65	0.52	0.74	0.48	0.68	0.79
P_2O_5	0.08	0.07	0.09	0.07	0.09	0.12
H_2O	0.30	0.40	0.26	0.25	0.30	0.10
CO_2	23.10	25.30	23.14	27.15	24.70	23.00
Total	98.88	99.35	98.58	99.10	98.97	98.52
ppm						
F	2581	3236	2558	2773	2845	2502
Ba	85	60	106	69	95	116
Rb	29	12	34	23	30	37
Sr	659	838	703	762	776	698
Zr	60	29	74	49	51	74
V	26	<10	36	18	33	39
Cr	69	61	70	60	75	79
Ni	12	10	14	12	14	15
Co	16	20	18	22	21	17
Zn	26	26	30	23	45	33